Spatial and temporal variability of Atlantic Water in the Arctic from forty years of observations

Alice E. Richards[1], Helen L. Johnson[1], Camille Lique[2]

[1]Department of Earth Sciences, University of Oxford, Oxford, United Kingdom
[2]Université de Bretagne Occidentale, CNRS, IRD, Ifremer, Laboratoire d'Océanographie Physique et Spatiale, IUEM, Brest, France

Key Points:

- Atlantic Water is evolving in opposing ways in eastern and western sectors
- Data suggest Atlantic Water cools during transit via vertical mixing at its upper bound and through interaction with cool dense shelf waters
- Atlantic Water core temperature is generally effective in assessing Atlantic Water heat content but does not always capture temporal trends

Corresponding author: Alice Richards, `alice.richards@stx.ox.ac.uk`

Abstract

Atlantic Water (AW) is the largest reservoir of heat in the Arctic Ocean, isolated from the surface and sea-ice by a strong halocline. In recent years AW shoaling and warming are thought to have had an increased influence on sea-ice in the Eurasian Basin. In this study we analyse 59000 profiles from across the Arctic from the 1970s to 2018 to obtain an observationally-based pan-Arctic picture of the AW layer, and to quantify temporal and spatial changes. The potential temperature maximum of the AW (the AW core) is found to be an easily detectable, and generally effective metric for assessments of AW properties, although temporal trends in AW core properties do not always reflect those of the entire AW layer. The AW core cools and freshens along the AW advection pathway as the AW loses heat and salt through vertical mixing at its upper bound, as well as via likely interaction with cascading shelf flows. In contrast to the Eurasian Basin, where the AW warms (by approximately 0.7 °C between 2002 and 2018) in a pulse-like fashion and has an increased influence on upper ocean heat content, AW in the Canadian Basin cools (by approximately 0.1 °C between 2008 and 2018) and becomes more isolated from the surface due to the intensification of the Beaufort Gyre. These opposing AW trends in the Eurasian and Canadian Basins of the Arctic over the last 40 years suggest that AW in these two regions may evolve differently over the coming decades.

Plain Language Summary

A few hundred meters beneath the surface of the Arctic Ocean lies a warm, salty layer of Atlantic origin, called Atlantic Water (AW), which is isolated from sea-ice and the ocean surface by a vertical salinity gradient that acts as a barrier between the AW and the surface. In recent years, weakening of this barrier and warming of AW in the eastern Arctic have contributed to unprecedented sea-ice loss. This study analyses 59000 vertical temperature and salinity profiles from the Arctic Ocean from the 1970s to 2018 to obtain a broad picture of the AW and its variability. The AW temperature maximum is found to be an easily observable, generally effective way to assess how much heat is stored in the AW layer. Over the period studied, the AW in the eastern Arctic warmed and had an increasing influence on the amount of heat in the surface layer, whereas AW heat became increasingly isolated from the surface in the west due to changes in local winds. The emergence of a characteristically different eastern and western Arctic Ocean in the future could have important consequences, both in terms of Arctic sea-ice loss and global ocean circulation.

1 Introduction

Beneath the cool, fresh surface layer of the Arctic Ocean lies a warm, saline intermediate layer of Atlantic origin. This Atlantic Water (AW) flows in through the Fram Strait (as the Fram Strait Branch) and the Barents Sea (as the deeper, cooler Barents Sea Branch) and travels cyclonically around the Arctic as a topographically steered boundary current following the continental slope, with part of the current recirculating along the Lomonosov and Alpha-Mendeleev Ridges into the interior and back towards the Fram Strait (Aksenov et al., 2011; Woodgate et al., 2001). It eventually exits the Arctic into the North Atlantic via the Canadian Arctic Archipelago (CAA) and the Fram Strait, fresher and cooler than it came in, having taken about 20-30 years to complete its journey (Lique et al., 2010; M. J. Karcher & Oberhuber, 2002; Rudels, 2015; Wefing et al., 2020). Heat is transferred from this AW boundary current to the interior via intrusions and eddies (McLaughlin et al., 2009; Kuzmina et al., 2011).

The AW layer is the most significant reservoir of heat in the Arctic Ocean (Carmack et al., 2015), therefore changes in its temperature could have a significant impact on the Arctic region. The AW layer currently contains enough heat to melt all Arctic sea-ice within just a few years if this heat were brought to the surface in that time (Turner, 2010),

although across most of the Arctic the AW is isolated from the sea-ice and surface mixed layer by a strong halocline. Observations suggest that AW temperature variations are dominated by low-frequency oscillations with a period of 50-80 years, linked to changes in the Nordic Seas which are advected through the Fram Strait (Polyakov et al., 2004). Superimposed on these low-frequency oscillations are inter-annual pulse-like temperature variations which enter through the Fram Strait or St Anna Trough and are advected with the boundary current (M. J. Karcher et al., 2003; Schauer et al., 2002; Dmitrenko et al., 2008; Polyakov et al., 2004; McLaughlin et al., 2009). There was also a net warming trend in AW temperature over the twentieth century (Polyakov et al., 2004, 2012), and AW in the Fram Strait is now unprecedentedly warm compared to the last two millennia, with a rapid temperature increase in the upper AW layer over the last 120 years (Spielhagen et al., 2011).

In the eastern Eurasian Basin, recent increases in AW temperature, along with associated shoaling of the AW and a weakening halocline, have enhanced vertical heat transfer from the AW to the surface layer and have resulted in a substantial reduction in winter sea-ice formation (Lind et al., 2018; Polyakov et al., 2010, 2017). This "Atlantification" of this region shows how important a role AW can play in a changing Arctic. Furthermore, Atlantification and resultant sea-ice reduction can affect the AW itself in a variety of ways. The reduction of sea-ice import to the Barents Sea can cause a local increase in AW temperature, salinity, and hence density (Barton et al., 2018) and can also result in local convection which has consequences for the AW layer downstream (Lique & Steele, 2012; Lique et al., 2018). In the Eurasian Basin, reduced ice cover and a resultant increase in ventilation is expected to cause local decreases in AW temperature and salinity (Pérez-Hernández et al., 2019). The impact of these local AW changes on the wider Arctic region is not yet fully understood, but is another important part of the changing role AW can play in the future Arctic environment.

Downstream in the Canada Basin the impact of AW on sea-ice is currently observable at the margins of the Canada Basin, with AW upwelling here (caused by wind) linked to local sea-ice reduction (Ladd et al., 2016). Changes in both sea-ice cover and the intensity of the Beaufort Gyre in the interior Canada Basin can affect the AW (Lique & Johnson, 2015; Lique et al., 2015). The recent spin-up of the gyre resulted in a deepening of the underlying AW due to Ekman pumping, and a shoaling of the AW temperature maximum at the gyre margins (Zhong & Zhao, 2014). The pathway and intensity of AW in the Canada Basin are affected by the surface circulation here as well (M. Karcher et al., 2012; Lique et al., 2015).

Changes to the AW also have consequences outside of the Arctic. It is thought that the low density of the present warm AW anomalies in the Arctic could be maintained throughout their circumnavigation of the Arctic Ocean, and hence reduce the density of outflows into the North Atlantic (M. Karcher et al., 2011). The properties of the boundary current and these deep outflows that are advected into the North Atlantic have the potential to significantly influence overturning in this region - an important component of the global climate system.

Understanding how AW heat is likely to change in the future is therefore a key part of predicting what will happen to the Arctic in the years to come. There is large discrepancy and bias amongst coupled climate model representations of AW in the Arctic, with the AW layer generally being too deep and thick. The AW temperature biases are primarily due to inaccurate representation of sea ice coverage and surface cooling in the Barents Sea, formation of cold and dense water in the Barents Sea, and AW inflow temperatures through the Fram Strait (Shu et al., 2019; Ilıcak et al., 2016). It is therefore particularly important to have an observational description of AW to help evaluate these models, given their use in predicting future Arctic changes.

Oceanic observations in the Arctic are sparse and often seasonally biased, and many observational studies of the Arctic focus on specific regions or transects (e.g. Anderson et al. (1994); Beszczynska-Moller et al. (2012); Li et al. (2020); Lind et al. (2018); McLaughlin et al. (2009); Polyakov, Rippeth, et al. (2020)). However, the number of Arctic Ocean observations has increased in recent years. This study aims to synthesise data from various sources across the Arctic from the 1970s to 2018 to give a pan-Arctic, up-to-date description of the AW layer and its impact on the water column. Diagnostics derived from these observations, such as the temperature, salinity and depth at the AW temperature maximum (the AW core) and AW heat content are used to characterise the spatial and temporal variability of the AW and are described in section 2. The spatial variability of the AW properties is investigated in section 3, with temporal variability in both the eastern and western Arctic described in section 4. Observed changes in AW and heat distribution within the water column at moorings and at repeated CTD transects are discussed in section 5. Section 6 explores regional correlations between AW core metrics and vertically integrated AW layer properties to investigate both how representative the AW core temperature is of AW heat content, and regional differences in mixing. Conclusions are given in section 7.

2 Data and Methods

Conductivity-temperature-depth (CTD) observations from across the Arctic are used in this study, from four different sources: the ice-tethered profiler (ITP) program (Toole et al. (2011); Krishfield et al. (2008), `http://www.whoi.edu/itp`) and the Beaufort Gyre Exploration Project (BGEP, `https://www.whoi.edu/beaufortgyre`) - both based at the Woods Hole Oceanographic Institution - the Nansen and Amundsen Basins Observational System (NABOS, `https://uaf-iarc.org/nabos`), and data from the NOAA World Ocean Database (WOD, `https://www.ncei.noaa.gov/products/world-ocean-database`). The WOD collates oceanic observational data from a wide range of sources. The WOD data used here are those from CTD profiles, drifting buoys, and ocean stations. Any ITP, BGEP or NABOS data were removed from the WOD dataset before use to avoid duplication. The BGEP and NABOS datasets include data from both moorings and ship surveys.

Throughout the paper, salinity is given in Practical Salinity Units, and potential temperature (when not available directly from the observational data product), heat content and potential density are computed using the Thermodynamic Equation of Seawater 2010 (TEOS-10) (IOC et al., 2010).

All data used in this study are processed versions of the raw data gathered in the field. Details of these procedures can be found in the sources referenced above, but all involved calibration, sensor-correction and the removal or flagging of obviously erroneous data. In addition to this initial processing, further routines were applied to the data and profiles were smoothed for much of our analysis - details of which are given below. Profiles with more than 10 % of data masked or flagged as suspicious were omitted from the analysis and, unless otherwise stated, monthly mean data from moorings were used so as not to bias any regional analysis to the mooring locations due to the relative high sampling frequency here compared to other locations. This resulted in about 59000 profiles for analysis.

Here we define the Atlantic Water layer as that portion of the water column that lies below the halocline and has potential temperature above 0°C. The top and bottom of the layer are the 0°C crossing points, either side of the potential temperature maximum, and the AW layer thickness is the distance between them. As density is driven by salinity in the Arctic, potential temperature is effectively a passive tracer. The potential temperature maximum, referred to here as the AW core, is commonly used to fol-
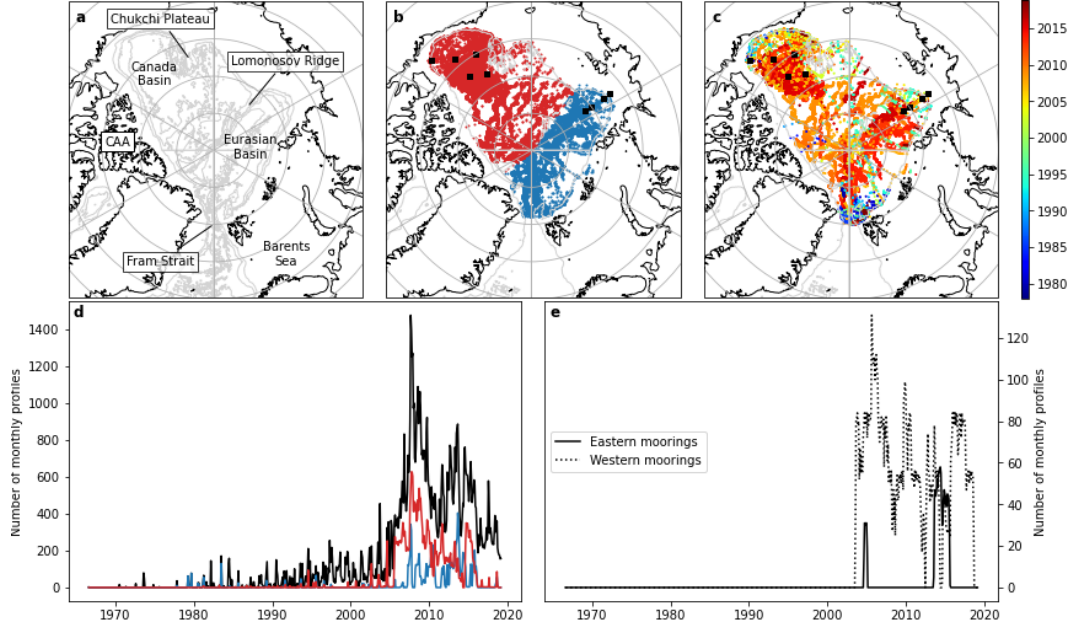
Figure 1. (a) Map of the Arctic with bathymetric contours for every 1000 m shown along with relevant geographic features. (b) Spatial distribution of all AW core data points coloured by region, with east in blue, west in red, and mooring locations marked with black squares. (c) Spatial distribution of all AW core data points coloured by the year in which the measurements were obtained. (d) Time series showing number of monthly profiles, with east in blue, west in red and all Arctic data in black (some of which lay outside of both the eastern and western regions, so are not shown on map or used in analysis). (e) Time series showing number of monthly mooring profiles in the eastern and western regions.

low the circulation and transformations of AW (M. J. Karcher et al., 2003), and is the focus of much of this manuscript.

The AW core in a given profile is defined as the point at which the maximum potential temperature is reached, in the portion of the profile with salinity greater than 34.7 (in order to avoid surface temperature maxima), following Lique and Steele (2012). Figure 1 shows the distribution in time and space of profiles where the AW core was identified, with mooring locations shown as black squares.

To ensure the AW core identified in each profile was not an artefact of limited sampling, profiles were required to start above 100 m and cover a depth range of at least 500 m before being used to identify the AW core (this also eliminated data from the surrounding shelf seas, allowing the study to focus on AW within the Arctic basin only). This latter step resulted in about 44000 AW core data points. Before identifying the core, profiles were smoothed over a vertical distance of 80 m by taking the mean of the profile data within 40 m of each data point. This length scale was chosen as it was the best at preserving the general shape and magnitude of the temperature profile, while removing the spikes due to features such as thermohaline intrusions and eddies (although please note that this smoothing was not applied to the profiles in Figure 3). This is important as the main aim of this study is to get a general picture of patterns and long-term trends in AW core properties, and features such as intrusions can disproportionately affect the depth of the AW temperature maximum in basin interiors in such a way as to detract

from this. Any profiles used in the analysis should be assumed to be smoothed unless stated otherwise.

The depth coverage varies between data sources - ITP profiles cover the upper 800 m of the water column, whereas many data from CTD stations and moorings extend down to around 2000 m. This variation in depth range does not affect the analysis in this study given that the AW core can be identified in both cases, and any profiles that do not sample the whole AW layer are omitted from the AW heat content analysis in sections 5 and 6. Although ITPs and moorings provide year-round measurements, there remains a spring/summer bias in data from other sources. However, this is unlikely to impact results due to the negligible seasonality of AW when compared to its overall variability in space and time (Lique & Steele, 2012).

Heat content, HC, was computed for various portions of the vertical temperature profiles according to

$$HC = \int_a^b \rho_\theta(z) c_p T(z) \, dz \qquad (1)$$

where ρ_θ (in $kg\,m^{-3}$) is potential density, c_p (in $J kg^{-1} \, °C^{-1}$) is specific heat, T (in $°C$) is potential temperature, z (in m) is depth, and a and b are the depth bounds defining the layer in question. Approximately 1500 profiles sampled the entire AW layer and allowed for the computation of total AW heat content. To account for differing profile lengths above the AW layer (due to variation in upper depths of profiles and the depth of the AW layer itself), heat content density is used to evaluate the heat stored in this upper layer in a similar way to Polyakov et al. (2011). The heat content derived for this upper portion of the water column is divided by the depth range over which it is computed. This quantity is proportional to the average temperature over that depth range.

3 The Atlantic Water core across the Arctic

Investigating how the hydrographic properties of the AW core change across the Arctic can give a good picture of the behaviour of the AW layer in general. Figure 2 shows maps of the potential temperature, salinity, depth and potential density anomaly of the AW core from all observations, giving an idea of the general spatial distribution of properties at the depth of the AW temperature maximum.

Figure 2b highlights the temperature difference between AW core properties in the Eurasian Basin and western Arctic. The core loses heat as it is advected around the basin - its temperature in the Canada Basin is approximately 1.5°C lower than where it is first subducted under the fresh surface layer at the southern boundary of the Eurasian Basin. The most significant heat loss is seen here, where, much like in the Nordic Seas (Lind et al., 2018), the AW loses heat to the atmosphere and through mixing with the cooler surface layer. The higher AW core temperature along the Lomonosov Ridge relative to the western Arctic boundary suggests that the AW that recirculates back along the ridge is warmer than that which continues towards the western Arctic.

The salinity of the core (Figure 2c) decreases on its journey around the Arctic, particularly in the Eurasian Basin where it mixes with fresher surface waters upon subduction. Turbulent mixing may play an important role in AW freshening in parts of the western Arctic - the difference in AW core salinity (and temperature) between the boundary and interior of the Canada Basin is indicative of this. Whereas the AW in the interior of the Canada Basin has travelled around the north of the Chukchi Plateau, the AW at the boundary has travelled over the Chuckchi Plateau's complex bathymetry (McLaughlin et al., 2009; Li et al., 2020). The relatively low temperature and salinity of this boundary AW can be explained by enhanced mixing experienced over this rough topography upstream.
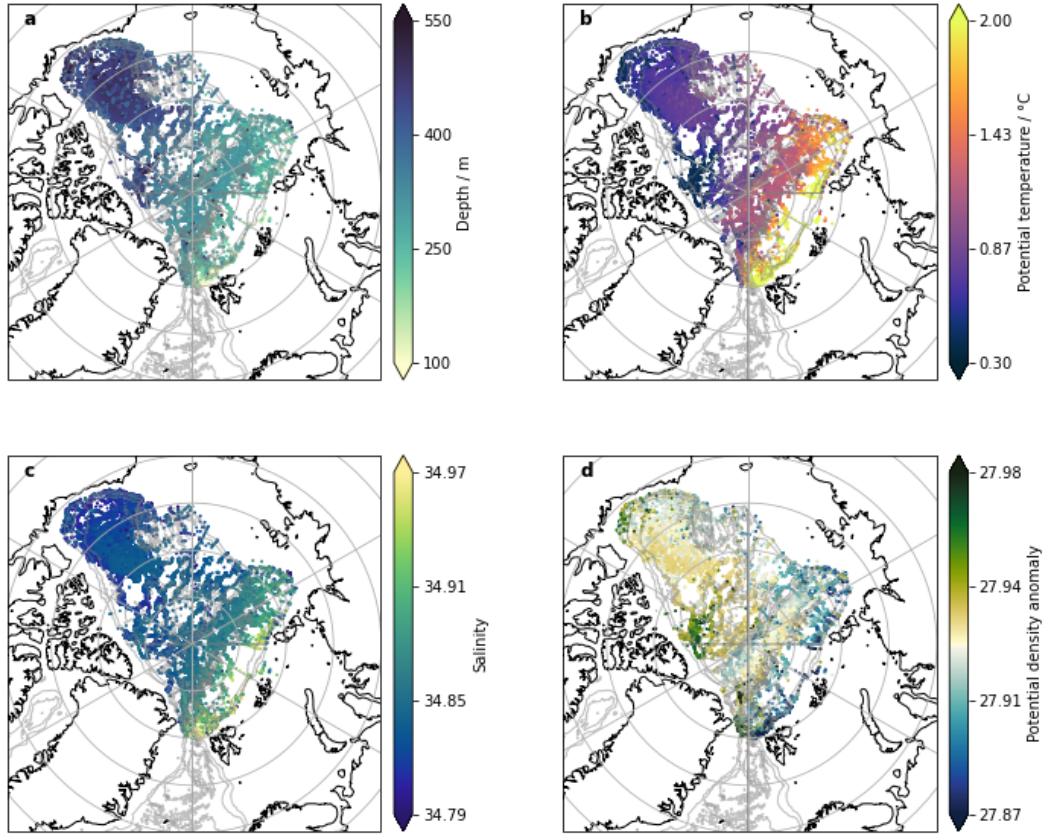
Figure 2. Maps showing (a) depth (b) potential temperature (c) salinity and (d) potential density anomaly of all AW core data points used in this study.

Despite the AW core freshening along the AW advection pathway, the density of the core appears to increase from its relatively low value along the southern Eurasian Basin boundary to higher values in the western Arctic and Eurasian Basin interior (Figure 2d). There are particularly dense, cold regions along the western shelves just north of the Canadian Arctic Archipelago (CAA) and Greenland. This is surprising given the importance of salinity in governing density at such cold temperatures, but may be explained by heat loss from the top of the AW layer to the fresher, cooler water above through vertical mixing as AW is advected. This would deepen the AW core without the AW layer as a whole getting denser, as heat lost preferentially from the upper AW would result in the core being found on deeper (denser) isopycnals. This could explain the cooling, freshening and increase in density of the AW core seen along the AW advection pathway, with the coldest and densest regions towards the end of its journey (Aksenov et al., 2011).

Another process which might be contributing to the cooling and freshening of the AW core during its advection is interaction between AW and cold, dense cascading flows from the shelves (formed from brine rejection during sea-ice formation). These flows have been modelled throughout the Arctic (Luneva et al., 2020), and have been observed to interact with and modify AW in the Eurasian Basin (Ivanov & Golovin, 2007). Observations of this interaction in the western Arctic are limited due to the sparsity of observations in these shelf regions, but dense water cascades have been observed to interact with waters as deep as the lower halocline here (Ivanov et al., 2004; Melling & Moore, 1995; Luneva et al., 2020), suggesting that interaction with upper AW is feasible.

Due to limitations in our dataset, we are unable to quantify the relative importance of these two potential mechanisms through which the properties of the AW core are modified. Although observational evidence of interaction between shelf flows and AW is limited in the western Arctic, it is likely that both heat loss from the top of the AW layer and interaction with shelf flows contribute to the AW core becoming cooler and denser along the AW advection pathway.

The AW core depth exhibits a bimodal structure, as shown in Figure 2a, being much deeper in the Canada Basin (approx. 500 m) than the Eurasian Basin (approx. 300 m) due to the Ekman pumping associated with the winds which drive the Beaufort Gyre. The effect of the Beaufort Gyre on the AW in the Canada Basin can also be seen in the (un-smoothed) vertical temperature profiles in Figure 3, where the cool waters of the gyre push down the AW layer to a much greater depth than that at which it resides in the eastern Arctic. However, the important role that the halocline plays in isolating the AW from the surface can be observed across the whole Arctic (see Figure 3).

Zig-zags and staircase features in these un-smoothed profiles also indicate the presence of thermohaline intrusions and diffusive convection, respectively (Bebieva & Timmermans, 2017). Thermohaline intrusions form in the presence of temperature and salinity gradients along isopycnals (Ruddick, 1992), and are an important mechanism for AW transport from the boundary to the interior of both the Canada and Eurasian Basins (McLaughlin et al., 2009; Kuzmina et al., 2011). They are often found near the AW core depth (unlike staircases which tend to be found above the AW core depth where diffusive convection is supported (Bebieva & Timmermans, 2019)). These intrusion signatures are seen in Canadian Basin data in the 2000s. Intrusions are also seen in the Eurasian Basin throughout the time period covered in this study, providing strong evidence for their long-term presence in this region, although they have been seldom documented beyond the Canadian Basin in previous studies.
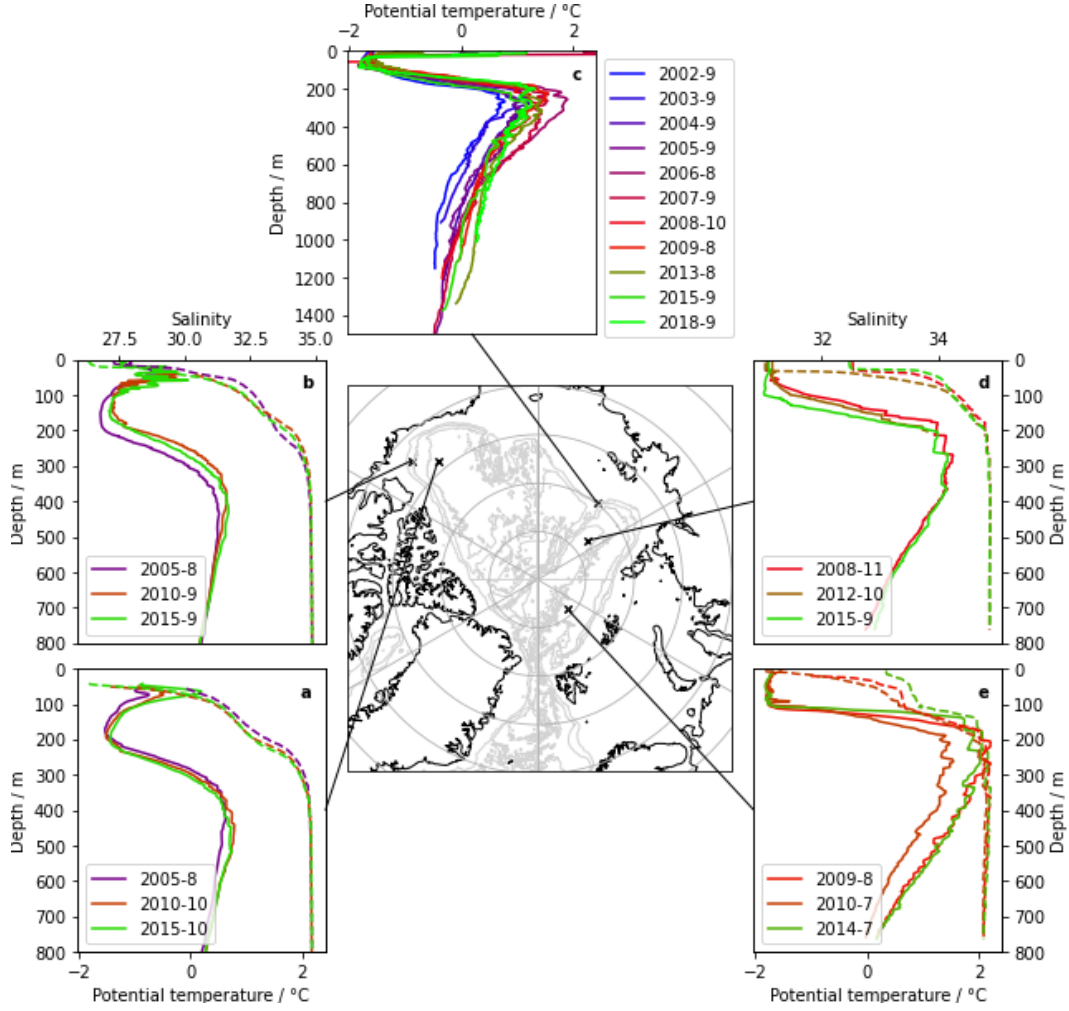
Figure 3. Un-smoothed potential temperature (solid) and salinity (dashed) profiles (a) in Canada Basin interior, (b) on Canada Basin shelf, (c) at the Siberian end of Lomonosov Ridge, (d) in the eastern Eurasian Basin, and (e) in the western Eurasian Basin. Profiles are coloured by the year in which they were measured, with year and month given in the legend. Note the change in y-axis scale in (c).

4 Regional differences in Atlantic Water properties and their temporal variability

Although the maps in Figure 2 give an idea of the general spatial variability of AW, they do not indicate how the AW has changed over the time period studied. This section will explore the temporal variability observed in the AW layer in different regions of the Arctic.

Figure 3 shows profiles from the same locations measured in different years. The uppermost plot in Figure 3 uses profiles from moorings at the Siberian end of the Lomonosov Ridge, sampling the AW boundary current. The depth range sampled by the moorings captures both AW branches - the Fram Strait Branch Water (FSBW) and the Barents Sea Branch Water (BSBW), centered at around 200-500 m and 750-1000 m, respectively. The temperature of these two branches here appears to vary independently in time. The BSBW shows a general warming trend throughout the period sampled (although this conclusion is tentative as we cannot rule out an influence of transient features such as eddies). This warming could hint at a more systematic change in BSBW temperature, which could be explained by surface air temperature increases over the Barents Sea (Skagseth et al., 2020) or reductions in sea-ice import to the region (Lind et al., 2018). The FSBW temperature is more variable from year to year, reflecting the variability of AW inflow temperature through the Fram Strait (Ivanov et al., 2012), although local transient features may also play a role in these profile differences. The heat loss experienced by the AW in the Barents Sea may act as a buffer for BSBW against high-frequency variation in upstream AW temperature.

Building on the regional differences in AW shown in Figure 2, Figures 4–7 highlight how the properties of the AW core in the eastern (blue) and western (red) Arctic evolve with time. Canada Basin mooring data is shown in black. Maps and annual normalised histograms show how the potential temperature, salinity, potential density anomaly and depth of the AW core change. The period covered by each map is indicated by grey lines enveloping the corresponding annual histograms - these periods were chosen to account for the varying amount of data available during each period. The reader is referred to Figure 1 for time series of the amount of data available from each region.

The year-to-year spatial variation in data distribution in the eastern Arctic makes inferring any trends from the histograms for the eastern Arctic difficult, and no significant trend can be found. After applying our processing scheme for core detection, only three years of eastern Arctic mooring data provides information on AW core properties (see Figure 1), so no meaningful trends can be identified from this fixed-point data either. However, the more consistent spatial distribution of data in the western Arctic and long time-series from mooring data allow trends to be inferred for the Canada Basin - these are described in more detail in the next section of this paper. The differences in the range of temperature and salinity data between the east and west highlights the transformation undergone by the AW as it travels around the basin, reinforcing what was shown in Figure 2, with AW core salinity and temperature decreasing due to mixing, and AW core density increasing.

The mooring data in Figure 4 reveal a gradual cooling in the Canada Basin after 2002, presumably after the arrival of the AW core warm temperature anomaly which entered the Canada Basin in the early 2000s (after having entered the Arctic through the Fram Strait in 1990) McLaughlin et al. (2009); Li et al. (2020). The maps in Figure 4 show the spread of this anomaly from the northern edge of the Chukchi Plateau into the interior of the Canada Basin in 2000–2004, with a more homogeneous AW core temperature field in 2005–2009.

Figures 5, 6 show an increase in AW core salinity and density in the interior of the Canada Basin throughout the mooring time period (2003–2018). This could be a down-
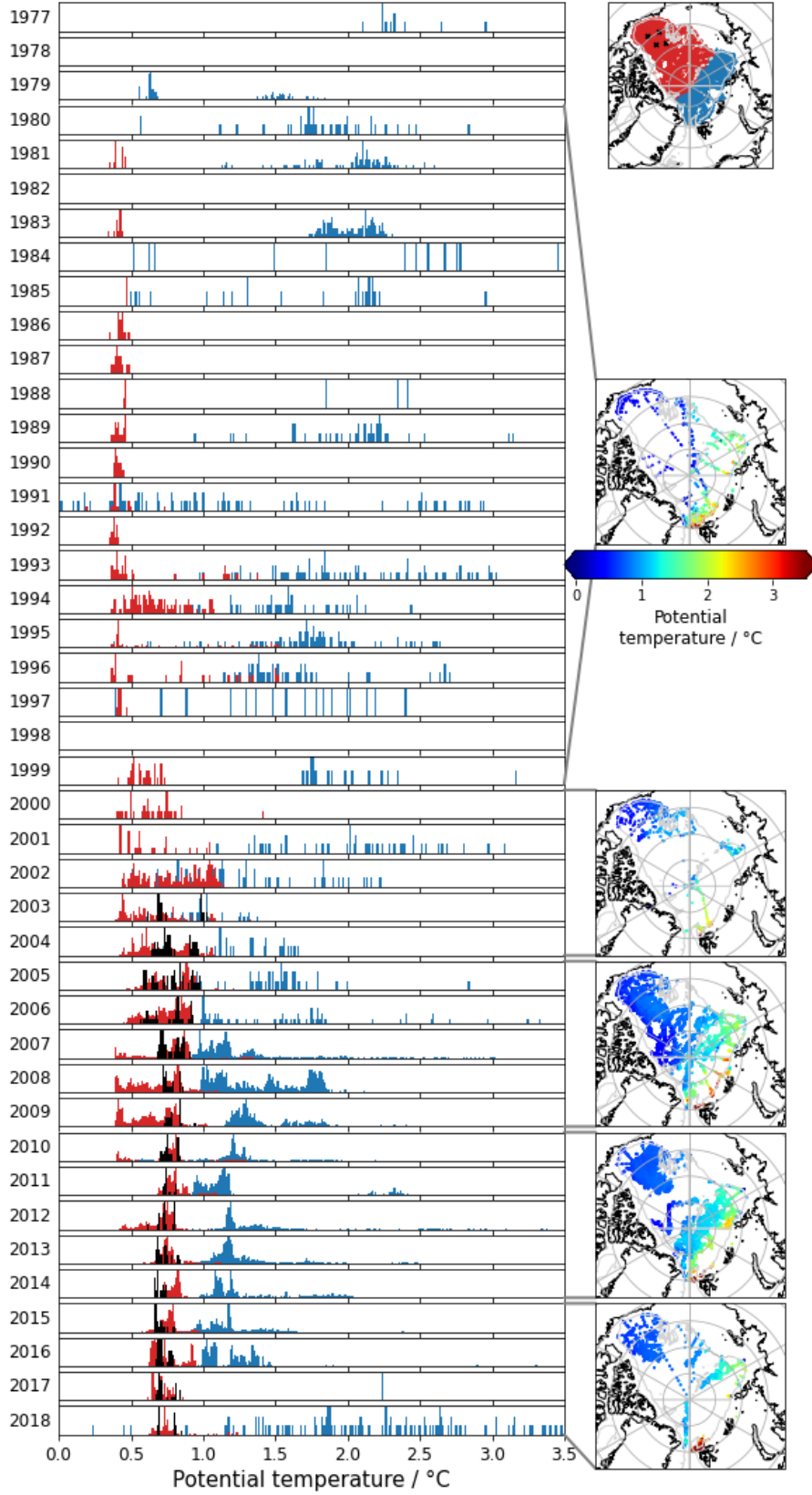
Figure 4. Annual normalised histograms of AW core potential temperature. Histogram data is coloured by region, with blue for eastern data, red for western data, and black for western mooring data - as shown in the map at the top right. The remaining maps on the right show the spatial distribution of the data in the histograms contained within each pair of grey lines.
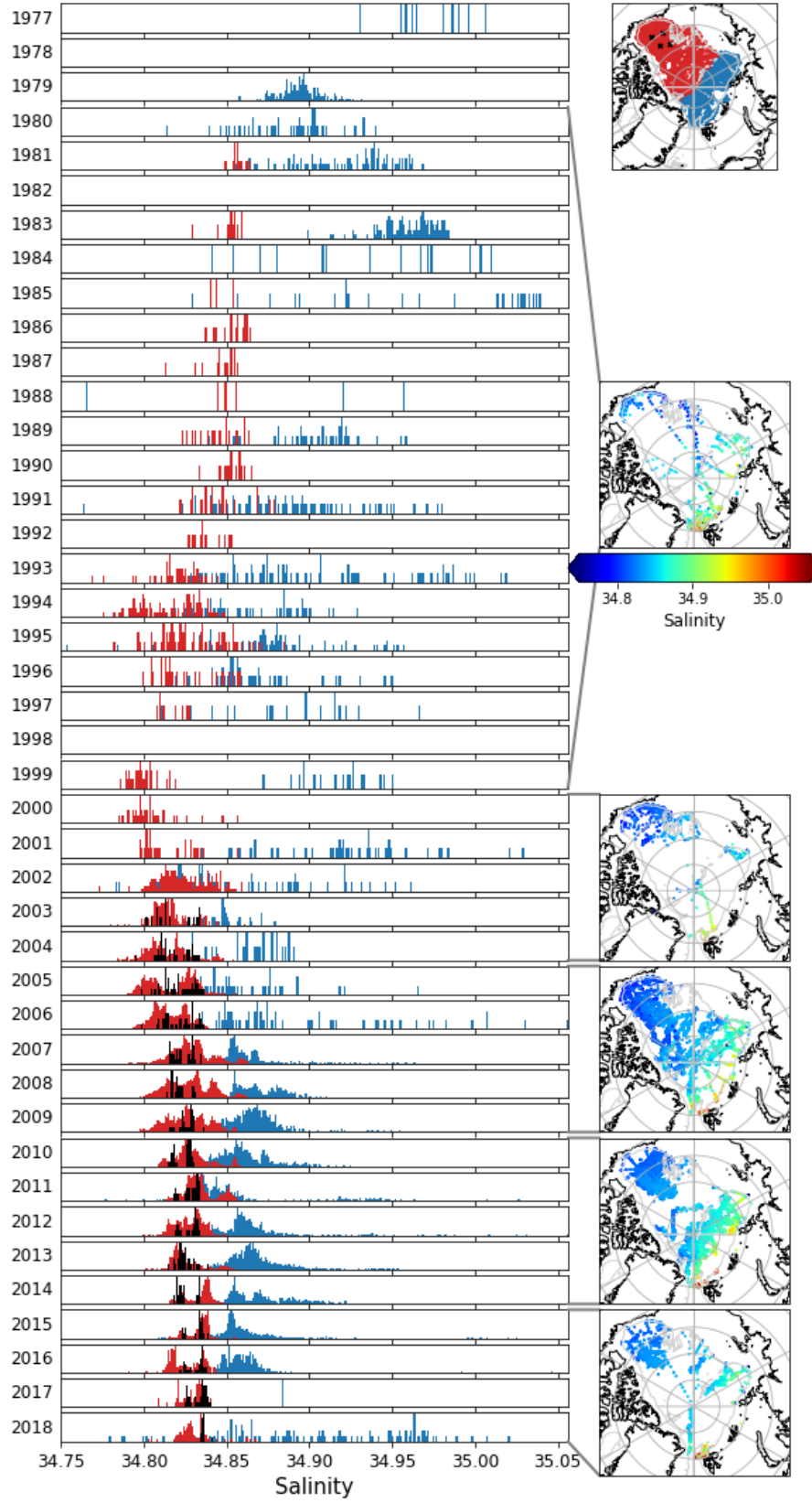
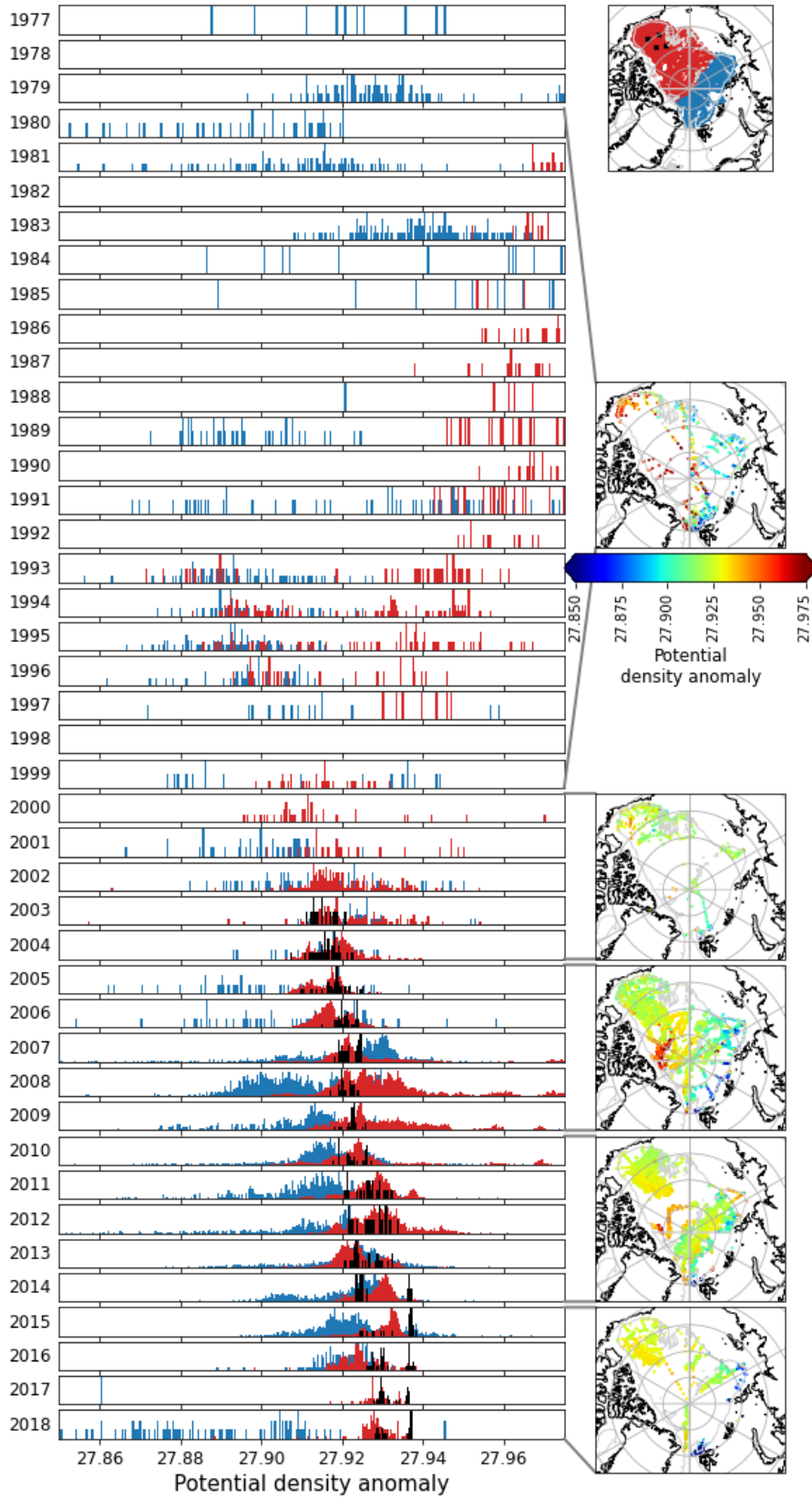**Figure 5.** As Figure 4 for AW core salinity

.

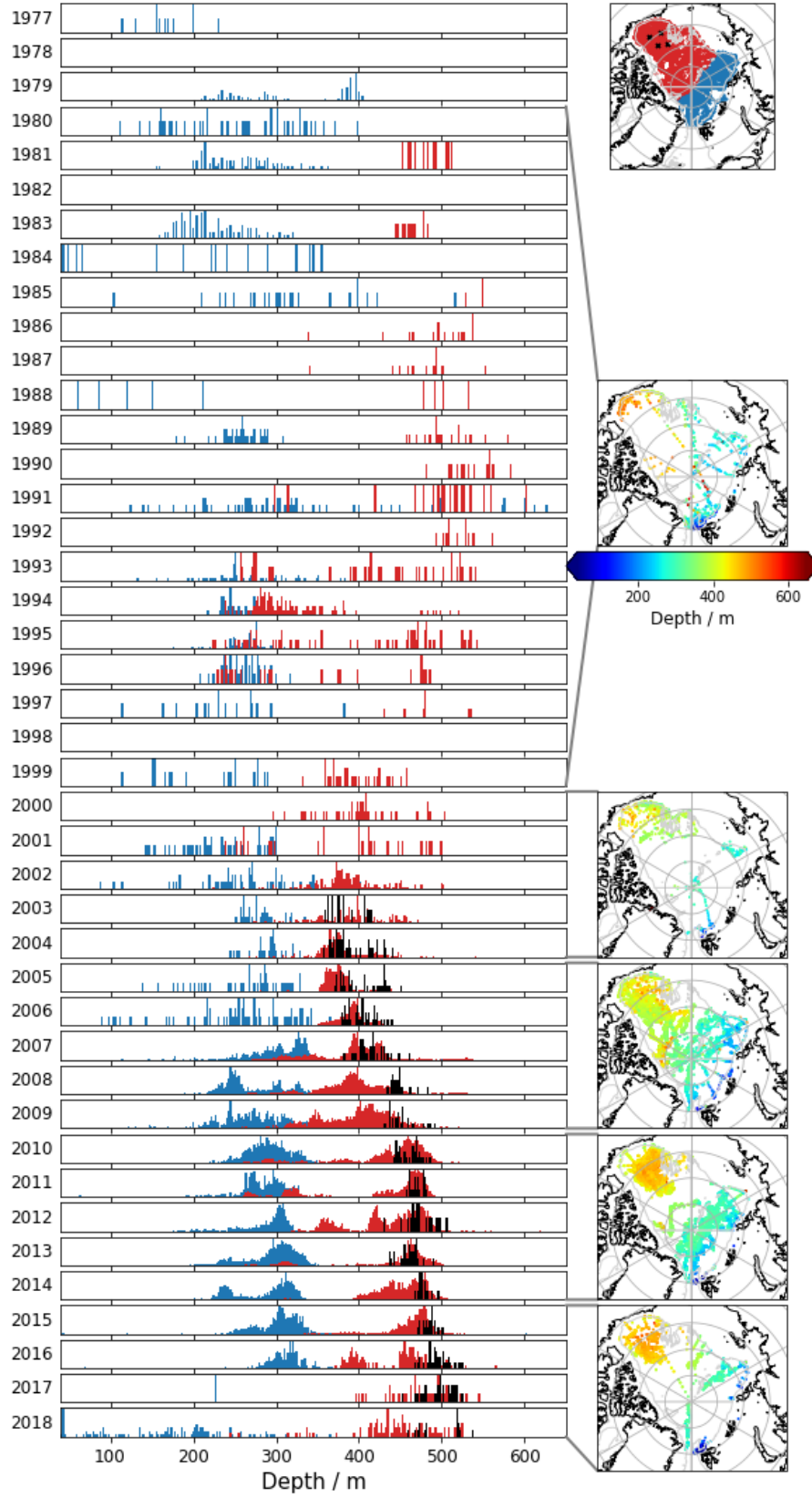**Figure 6.** As Figure 4 for AW core potential density anomaly

.

Figure 7. As Figure 4 for AW core depth

.

stream impact of Eurasian Basin Atlantification. Local increases in AW salinity in the Eurasian Basin and surrounding seas due to reduced Eurasian Basin sea-ice have been documented (e.g. (Lind et al., 2018; Barton et al., 2018)), but the impact of these changes on AW downstream in the western Arctic is not yet fully understood.

Alternatively, an increase in the AW core salinity and density within the Canada Basin could be due to the AW core moving deeper as heat is transported away from it. Unlike at the boundary, where turbulent mixing (McLaughlin et al., 2009; Li et al., 2020) results in similar changes in AW core temperature and salinity, in the interior diffusion governs the vertical transport of temperature and salinity. The diffusive convection regime in the upper AW layer (Bebieva & Timmermans, 2019) results in temperature being diffused more effectively than salt, causing the core to cool but not freshen. The warmest point is then located at a deeper, more saline part of the AW.

The most prominent trend in these histograms is the increasing depth of the AW core in the Canada Basin mooring data (Figure 7). Zhong and Zhao (2014) showed that the AW deepening caused by the spin up of the Beaufort Gyre dominates over the influence of AW core density on depth if the gyre intensifies sufficiently, with AW position in relation to the gyre centre becoming more important than its density from 2007 onwards. This means that when the gyre is sufficiently intense, AW suppressed by the gyre can reside deeper than other AW that is denser (e.g. that at the Canada Basin boundary which the gyre does not suppress). Figure 7 shows that the deepening of the AW core coincides with the isopycnal deepening reported by Zhong and Zhao (2014), Proshutinsky et al. (2019) and others. The effect of the AW core potential density increase on this core deepening will be investigated in the following section of this paper, where the whole water column will be considered.

5 AW variability at transects and moorings

Broad regional trends in AW core properties have been discussed above. To investigate these further, and put AW core property changes within the context of the wider water column, the temporal variability of data at moorings and across regularly repeated CTD transects is investigated below. This reveals more about the implications of AW changes for water column stratification and heat distribution. Trends from individual Canada Basin moorings (black data in Figures 4–7) are also discussed in more detail.

5.1 Eurasian Basin

The potential temperature and salinity along a NABOS CTD transect repeated from 2002–2018 across the AW boundary current in the eastern Eurasian Basin is shown in Figure 8. The year of each transect is given in the plot, and the AW core depth is identified with a black dot. The vertical black lines near the surface of the transects show the location of the CTD profiles. Data between these profiles have been interpolated using a Delaunay triangulation grid. The AW layer warms in general throughout the time period (when comparing the start and end years). However, this warming is pulse-like rather than continuous, with one warm pulse peaking in 2007–08 (likely the same warm pulse of AW that entered through Fram Strait around the year 2000 (Polyakov et al., 2005, 2011)) and a second in the 2018 section. The AW core in 2018 is 1°C warmer than that in 2002. The salinity of the AW also shows an increasing trend throughout the time period covered in Figure 8, although regions and years of high salinity are not coincident with regions or years of high temperature.

Figure 9 allows for a more quantitative assessment of the changes in the water column at this location. The first three panels of this figure show the evolution of AW core properties across the transect. This figure shows more clearly that the core freshens onshore in most years, suggesting that AW is mixing with fresher waters from the shelf or
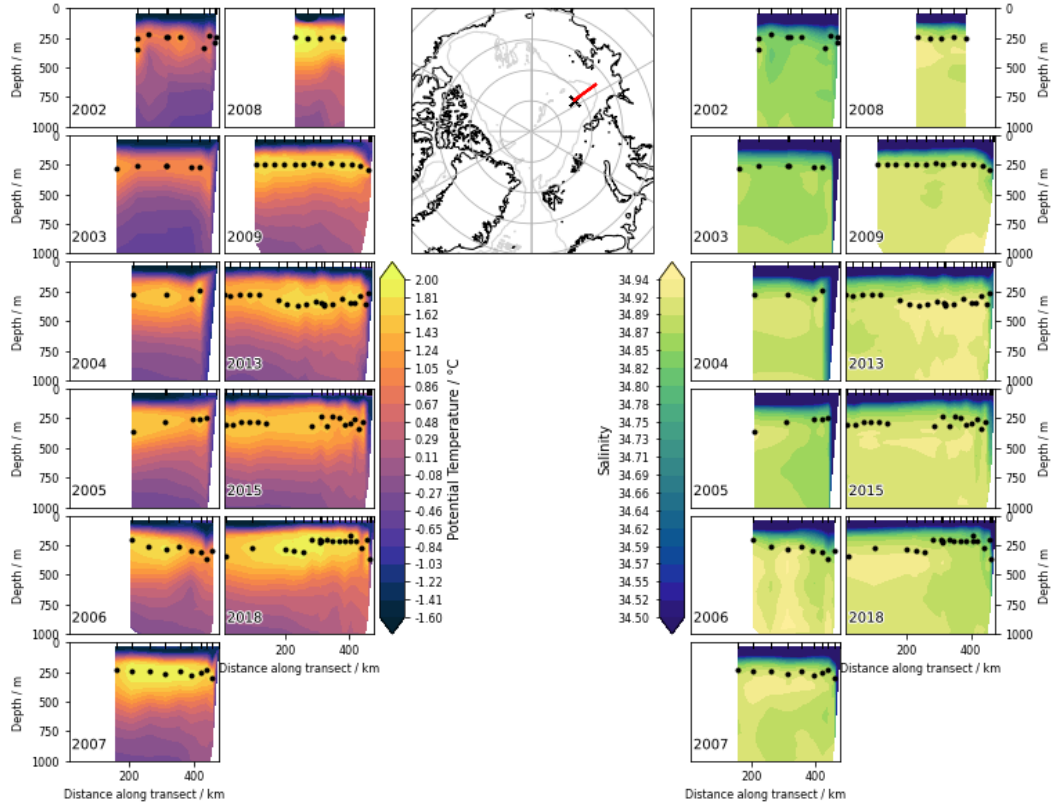
Figure 8. Potential temperature and salinity along a repeated CTD transect in the eastern Eurasian Basin. The year in which each transect was taken is given at the bottom left of each plot. In all years, transects were measured in August, September or October. The origin of the x-axis of the transect is marked with a black cross on the map, so that the x-axis origin is at the most offshore station. CTD profile locations are marked on the transect plots with vertical black lines at the surface. The black dots on the transect plots denote the location of the AW core.
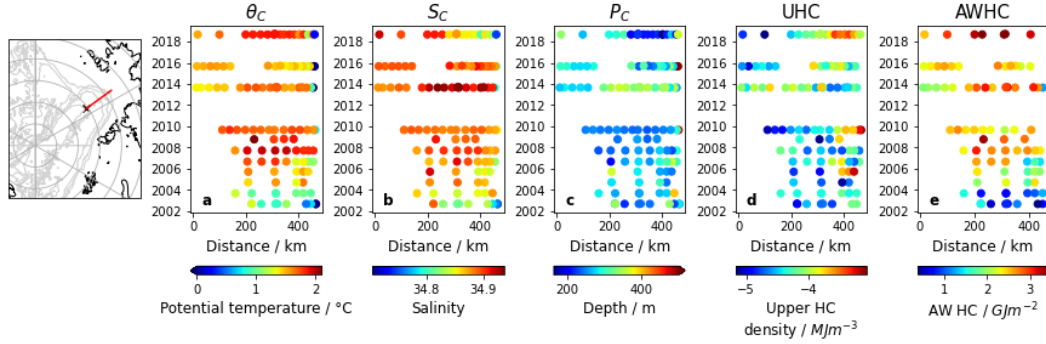
Figure 9. Water column properties across a repeated CTD transect in the eastern Eurasian Basin. Year markers denote the start of that year. Transect location is shown on the map, with a black cross denoting the x-axis origin of the transect plots. The x-axis origin is therefore at the most offshore station. Transect plots show (a) AW core potential temperature, (b) AW core salinity, (c) AW core depth, (d) heat content density of the water column above the AW layer, denoted as upper heat content (UHC), and (e) total heat content of the AW layer.

that the AW that reaches the shelf is that which is fresher. As above, the core temperature (and AW layer heat content shown in panel five) exhibits warm pulses which are superimposed upon a general warming trend across the period. Between 200-300 km along the transect, AW core temperature and salinity have linear trends of 4.13×10^{-2} °C per year (resulting in an increase of 0.7 °C between 2002–2018) and 3.63×10^{-3} psu per year, respectively. Nearer the boundary, greater than 350 km along the transect, these trends are reduced to 1.52×10^{-2} °C per year and 7.64×10^{-4} psu per year. This reduction in magnitude of AW core property trends away from the interior is likely due to enhanced mixing near the boundary. Notably the heat content of the AW layer increases to three times its 2002 value in 2018. The salinity and depth of these warm pulses differ, however - the AW core during the warm pulse in 2018 is fresher and shallower than the one in 2008. A weakened halocline may have allowed the warm AW to shoal higher in the water column and mix with the fresher surface layer, as reported by Polyakov, Rippeth, et al. (2020). The 2013 transect, although slightly cooler than those from 2008 and 2018, has a comparatively salty, deep AW core. This non-coincidence of AW core salinity and temperature changes suggests that even enhanced mixing due to a weaker halocline does not mask the signal of these warm AW pulses.

The fourth panel of Figure 9 shows the "heat content density" (the heat content of a portion of the water column divided by the height over which it is computed) of the sampled water column above the AW layer, denoted as upper heat content (UHC) in the figure. This quantity is proportional to the average temperature of the surface layer and halocline. UHC increases when the AW core salinity is low and AW core depth is shallow - perhaps an indication that a shallower AW layer transfers more heat to the halocline and surface layer. Despite the similarities in AW core temperature of the 2009 and late-2013 transects, the fresher/shallower core in 2009 coincides with a larger surface layer heat content density. This emphasises the strong link between halocline strength and the depth and salinity of AW. This is also highlighted in recent work by Polyakov et al. (2018), where halocline stability, quantified using density anomalies throughout the layer, is identified as a key climate change indicator in the region. The implication that AW shoaling is more influential than AW temperature change on surface layer heat content is not surprising given the low levels of vertical mixing throughout the Arctic (Fer, 2009). This
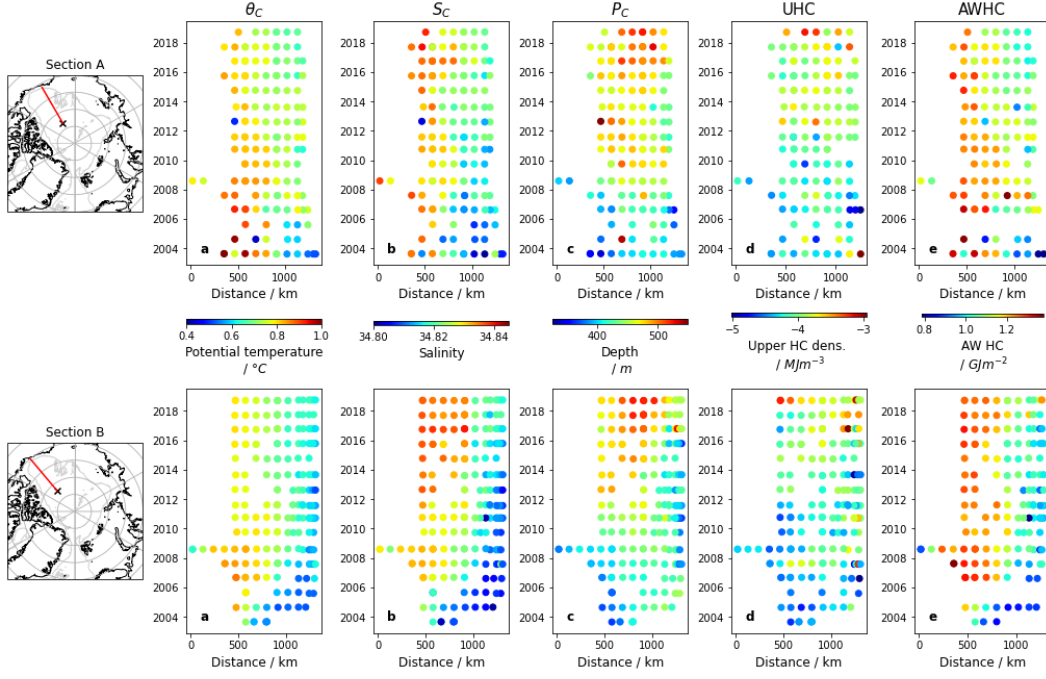
Figure 10. Water column properties across two repeated CTD transects in the Canada Basin. Year markers denote the start of that of year. Transect location is shown on the maps, with black crosses denoting the x-axis origin of each transect. The x-axis origin is therefore at the most off-shore station. Remaining panels show (a) AW core potential temperature, (b) AW core salinity, (c) AW core depth, (d) heat content density of the water column above the AW layer, denoted as upper heat content (UHC), and (e) total heat content of the AW layer.

is also reflected in the dissimilarity between variations in AW layer heat content and UHC seen in Figure 9.

5.2 Canada Basin

Figure 10 shows the same analysis applied to two repeated CTD transects in the Canada Basin. This allows for detection and comparison of any signals advected downstream from the Eurasian Basin transect in Figure 9. The length of the transects also enables comparisons between AW found on the boundary and within the interior of the Canada Basin.

As in the Eurasian Basin, Figure 10 shows evidence of the pulse-like nature of AW core temperature evolution, with warm AW core values in the interior in the mid-2000s indicative of the warm anomaly that arrived in the Canada Basin in the early 2000s (McLaughlin et al., 2009). As seen in Figure 2, AW at the Canada Basin boundary (>1000 km along section A, and the furthest few data points of section B) is cooler and fresher than that in the interior due to the enhanced mixing it experiences upstream over the rough bathymetry of the Chukchi Plateau (McLaughlin et al., 2009; Li et al., 2020). This enhanced mixing and cooling is the likely reason why the warm temperature anomaly is not seen at the boundary in Figure 10 - the temperature signal is much weaker there than it is in the interior.

On both transects, at the boundary, AW core temperature and salinity vary similarly, presumably because both of these properties are governed by the same mixing pro-
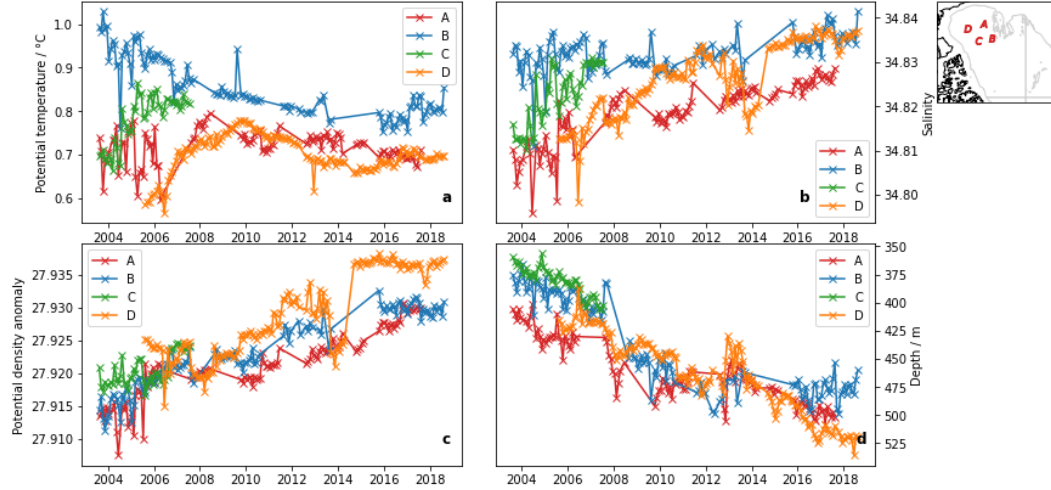
Figure 11. Time series of monthly mean AW core (a) potential temperature, (b) salinity, (c) potential density anomaly, and (d) depth from the four Canada Basin moorings. Mooring locations (A-D) are shown on the map at the top right.

cesses upstream. This is not the case in the interior, however, where from 2012 onwards both transects see an increase in AW core salinity which is not reflected in the temperature. This increase in salinity (and density) and decrease in temperature in the interior was also seen in the Figures 4–6. T-S plots of un-smoothed profiles from the ends of each annual transect (not shown here) reveal that the increase in interior salinity is accompanied by a disappearance of thermohaline intrusions i.e. the commencement of AW core cooling after the warm anomaly has arrived. This confirms the mechanism proposed earlier - of heat diffusing away from the AW core resulting in the core residing at a more saline part of the AW layer - as the most likely explanation for these trends. The idea that this AW core salinity increase is related to AW core heat loss, and is not related to changes in the AW layer as a whole, is also supported by a lack of trend in AW layer mean salinity in the Canada Basin interior over this period (not shown).

The slight warming in 2016 of the AW core temperature in the interior of section B of Figure 10 could be evidence of the AW warm anomaly observed upstream of the Chukchi Borderlands in 2010 (after having entered the Arctic Ocean through the Fram Strait around 2000, Li et al. (2020)). It can also be seen at the Eurasian Basin transect in Figure 9 around 2008, and until now has not been conclusively observed in the Canada Basin interior. This gives AW advection timescales from the eastern Eurasian Basin to the north of the Chuckchi Borderlands and around the north of the Borderlands into the Canada Basin interior of order 8 years, in agreement with other observational studies (Polyakov et al., 2011; Li et al., 2020). The amplitude of the warming is low compared to that of the previous warm temperature anomaly, despite the second anomaly being 0.24°C warmer than the first in the Eurasian Basin (Polyakov et al., 2010). This could be due to enhanced heat loss experienced by the AW during its advection, associated with increased ventilation, enhanced mixing with cooler, fresher water above, and/or interaction with shelf flows in the eastern Arctic (Ivanov & Golovin, 2007). Further observational data would be needed to confirm the presence of this second AW warm anomaly in the Canada Basin interior, however.

As discussed in Figures 4–7, the AW core in the Canada Basin cooled, freshened and deepened from the early 2000s onward. Trends from individual Canada Basin moorings (data in black in Figures 4–7) are more clearly shown in the time series in Figure

Table 1. Trends in monthly mean AW core potential temperature, salinity, potential density anomaly, and depth from each of the four Canada Basin moorings. R-squared values for the fit of each trend are given in parentheses. Note that mooring C data only cover five years (see Figure 11).

Mooring	θ trends / °C $year^{-1}$	Salinity trends / psu $year^{-1}$	σ_θ trends / $kgm^{-3}year^{-1}$	Depth trends / m $year^{-1}$
A	$2.81 \times 10^{-4}(0.00)$	$2.22 \times 10^{-3}(0.76)$	$1.79 \times 10^{-3}(0.88)$	$9.204(0.79)$
B	$-1.81 \times 10^{-2}(0.70)$	$6.90 \times 10^{-4}(0.26)$	$1.70 \times 10^{-3}(0.89)$	$12.24(0.82)$
C	$3.82 \times 10^{-2}(0.61)$	$4.74 \times 10^{-3}(0.70)$	$1.33 \times 10^{-3}(0.43)$	$9.80(0.79)$
D	$2.17 \times 10^{-4}(0.00)$	$1.96 \times 10^{-3}(0.73)$	$1.52 \times 10^{-3}(0.75)$	$9.01(0.88)$

11 and are given explicitly along with their R-squared values in Table 1. Again, the western AW core temperature and depth trends in Figure 11 and Table 1 oppose those expected from the Atlantification reported in the east.

As seen in the maps in Figure 4, the warm anomaly that entered the Canada Basin in the early 2000s spread into the interior from the Chukchi Plateau before cooling (McLaughlin et al., 2009). This is reflected in the consistent, significant cooling trend at mooring B (Figure 11 and Table 1), and the pre-2010 warming at moorings C and D (Figure 11). There is an increase in salinity at all moorings, with significant trends at moorings A, C and D. As discussed above, this seems to be related to the cooling of the core after the spread of the warm anomaly. The resultant increase in AW core density can be clearly seen in Figure 11, with significant trends at moorings A, B and D (note that C has a shorter time series). The trends in depth in both Figures 7 and 11 are also significant (Table 1), and could be attributed to the increase in AW core salinity. However, comparing the patterns of change in AW core depth and salinity in Figure 10 suggests that the salinity increase is not the most important driver of this depth increase. As discussed, the spin-up of the Beaufort Gyre and associated enhanced downwelling influences AW depth (Lique & Johnson, 2015; Lique et al., 2015; Zhong & Zhao, 2014), so the increase in core depth is likely explained by gyre intensification.

The Hovmöller plots in Figure 12 reveal more about the mechanisms behind the AW core deepening in the Canada Basin, and also help explain the increase in upper layer heat content density. This figure shows Hovmöller plots of potential temperature profiles from three of the BGEP moorings in the Canada Basin (mooring c having been omitted due to the shorter time series available there), with white lines marking isopycnal depths. The core depth varies in concert with isopycnal depth at all moorings, again emphasising that changes elsewhere in the water column, rather than those of the AW properties themselves, are likely driving AW depth changes here. The increase in AW core salinity/density does not appear to play an important role, as seen in Figure 10. With the exception of mooring D (which the gyre moved away from during the start of the period shown (Regan et al., 2019)), the isopycnals and hence AW deepen over the time period covered. The temporal pattern of this deepening is in agreement with previous papers (Proshutinsky et al., 2019; Zhang et al., 2016) and can be attributed to an overall increase in Ekman pumping (and hence freshwater content) in the central Canada Basin between 2003-2018 due to a combination of changes in sea-ice conditions and the strength of the Beaufort Gyre (Proshutinsky et al., 2019).

The increase in upper layer heat content density seen in Figure 10 can also be attributed to Beaufort Gyre intensification. Pacific Water is subducted into the halocline of the interior Canada Basin via isopycnals which outcrop in the Chukchi Sea (Timmermans et al., 2014). The increase in Ekman transport has therefore resulted in thicker Pacific
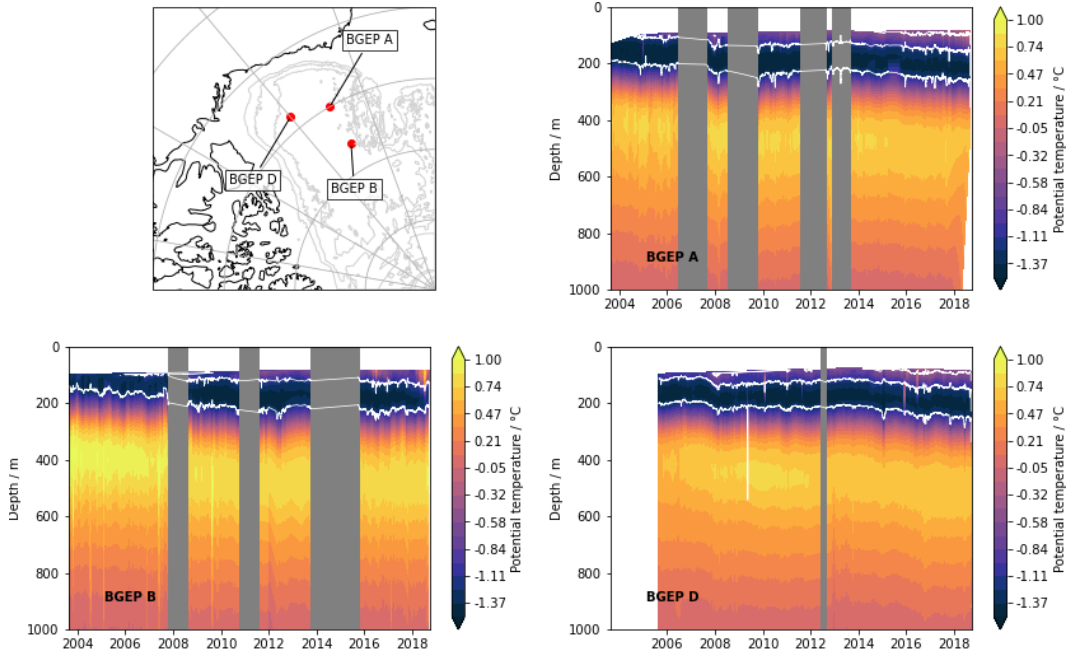
Figure 12. Hovmöller plots of potential temperature from three moorings in the Canada Basin (BGEP moorings A, B and D - locations shown on map). White lines denote the isopycnals - the deepest at 27 kgm^{-3}, contour interval 1 kgm^{-3}. Grey regions cover time periods with insufficient data.

Water layers within the Canada Basin halocline (Timmermans et al., 2014), and the warming of Pacific Summer Water (which can be seen as the warm shallow water mass that appears in later years of Figure 12) between 2003-2014 has subsequently resulted in an increase in halocline heat content (Timmermans et al., 2014, 2018). Changes in upper layer heat content density are therefore independent of AW heat content, as seen in Figure 10. This suggests that increases in sea-ice bottom-melt reported in the Beaufort Sea (Perovich & Richter-Menge, 2015) are likely due to Pacific Summer Water (along with other local features such as the near-surface temperature maxima (Jackson et al., 2012; Timmermans, 2015)), not AW warming. The deepening of the AW, and its increased isolation from the surface in the Canada Basin, is in stark contrast to the concurrent Atlantification seen in the Eurasian Basin.

Although spatial and temporal patterns of AW core potential temperature and AW layer heat content in Figure 10 are similar, they do not match as closely as might be expected. We explore this further in the following section.

6 Relationships between profile metrics

Much of the analysis in this study has involved the use of AW core properties to infer AW layer properties within the Arctic. It is therefore important to investigate how representative AW core properties are of the AW layer in general. Here we compute correlations between AW core and integrated AW layer metrics, which also shed some light on how the AW layer loses heat in each region.

The maps in Figure 13 show total AW layer heat content during different time periods, chosen to give a roughly even data distribution between panels. As most observational profiles do not sample deep enough to cover the entire AW layer, there are sub-
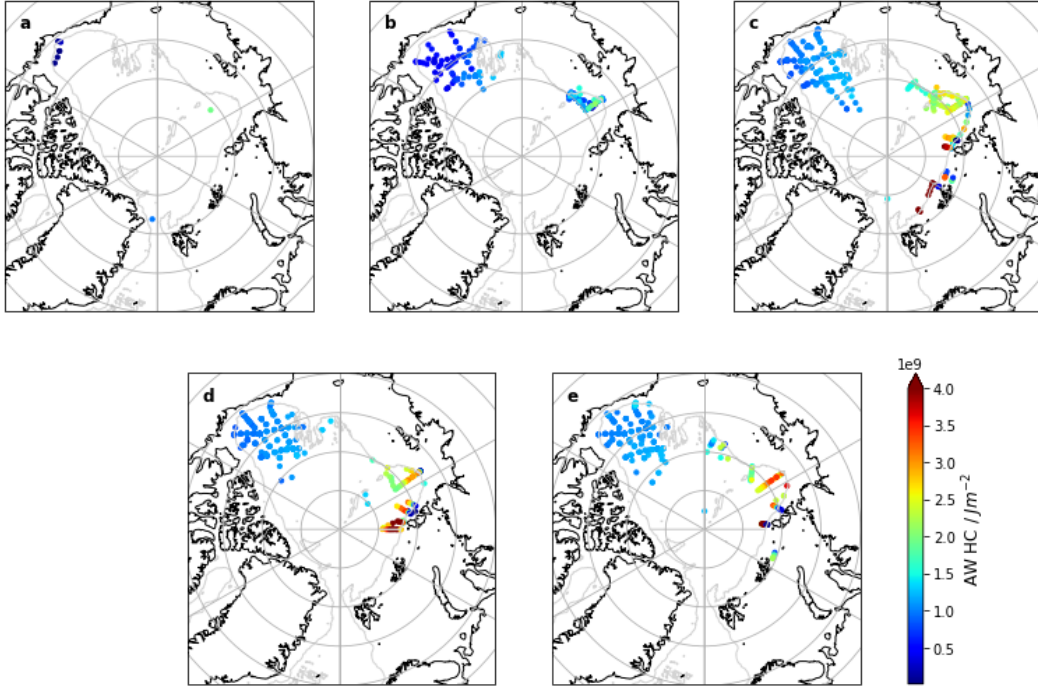
Figure 13. Maps of total AW layer heat content from all profiles which sampled the entire AW layer (defined as the layer between the two 0 °C crossing points either side of the AW core depth) for (a) 1980-1999, (b) 2000-2004, (c) 2005-2009, (d) 2010-2014, and (e) 2015-2018.

stantially less AW heat content data (1500 data points) than AW core data. This, of itself, emphasizes the usefulness of AW core data in assessing the pathways and evolution of the AW layer.

In the Canada Basin, total AW layer heat content increased in the mid-2000s (Figure 13, panels b to c) after the arrival of the AW warm anomaly (McLaughlin et al., 2009; Li et al., 2020) and has since remained at that higher level of approximately 1.5×10^9 Jm^{-2}, with no long term trend observed. The eastern Eurasian Basin (EEB) (i.e. the portion of the Eurasian Basin east of 90°E which has good data coverage for much of Figure 13) saw an increase in AW heat content throughout the period studied, in-line with the reported Atlantification of the region (Lind et al., 2018; Polyakov et al., 2010, 2017). Figure 13 shows a stark difference between AW heat content in the eastern Eurasian and Canada Basins, implying that the AW that bifurcates and recirculates towards the Fram Strait along the Lomonosov Ridge is warmer than the AW in much of the western Arctic. The heat content maps in Figure 13 are very similar to the AW core potential temperature maps in Figure 2, further suggesting that the AW core temperature captures the general pan-Arctic spatial pattern of AW heat content variability well. However, the cooling of the AW core in the Canada Basin (Figures 4 and 11) does not seem representative of the steady western AW heat content values in Figure 13, providing more evidence that the decrease in temperature (and increase in salinity) of the AW core do not reflect temporal changes in the AW layer itself.

To be more quantitative in assessing how well the AW core temperature represents AW heat content, correlations between these two metrics were computed. Figure 14 shows scatter plots between pairs of variables computed from profiles in both the eastern (restricted to EEB only due to constraints on spatial data coverage - see Figure 13) and western Arctic. These regions are defined in Figure 1. R-squared values for each of the plots
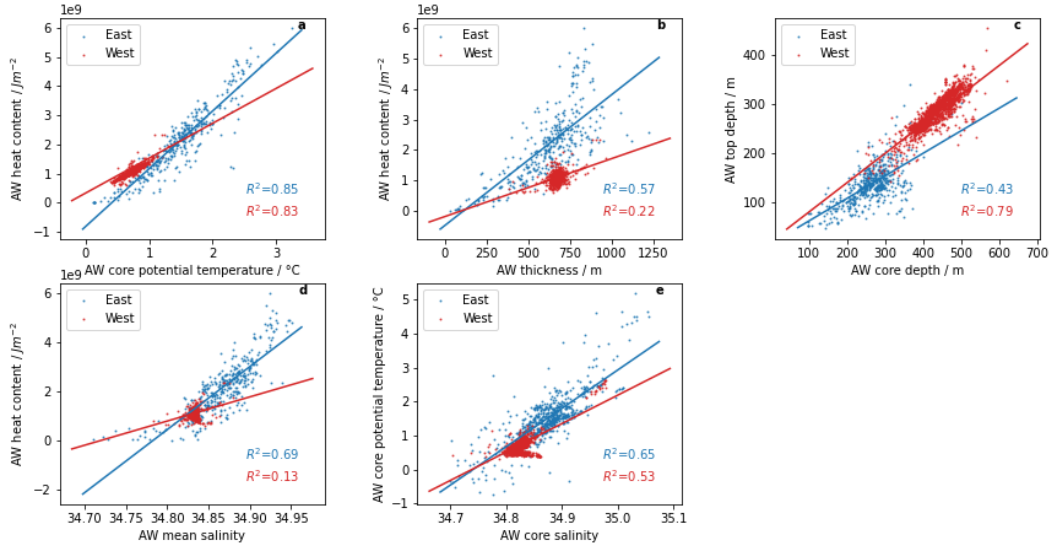
Figure 14. Scatter plots between (a) AW core potential temperature and total AW heat content, (b) AW layer thickness and AW heat content, (c) AW core depth and AW top depth, (d) AW mean salinity and AW heat content, and (e) AW core salinity and AW core potential temperature. Blue data is from the eastern Arctic, with red data from the western Arctic (regions defined in Figure 1). R-squared values and regression lines are shown for each scatter plot.

are given, along with regression lines. The relationship between total AW heat content and the potential temperature of the AW core is shown in Figure 14a. There is a strong correlation between these two variables in both the EEB and western Arctic, highlighting the general effectiveness of the AW core temperature as an easily measurable metric for assessing changes in AW heat content. As noted above, however, caution must be taken when using AW core properties to infer temporal trends in the AW layer, as the cooling (and resultant increase in salinity) of the AW core does not necessarily correspond with a cooling (or salinification) of the AW layer more generally.

Figure 14b shows AW layer thickness against AW layer heat content, with a moderate correlation in the EEB and a weak correlation in the west. This is an important reminder that although the potential temperature of the AW core will give a good idea of how AW heat content may vary (see Figure 14a), AW heat located away from the AW core also affects AW heat content. This is particularly true in the EEB where BSBW heat in the deep AW (which does not vary in concert with FSBW/the AW core, as seen in Figure 3) affects AW heat content.

Figure 14c shows the relationship between AW core depth and the depth of the upper boundary of the AW layer (i.e. the 0°C crossing point above the AW core depth). AW temperatures in both the eastern and western Arctic appear to be affected by heat loss from the top of the AW layer, causing the temperature maximum to deepen, although not necessarily to the same extent as the AW top (which is defined by a fixed temperature). This lowers the correlation between these two variables. However, there is a much stronger correlation in the west than in the EEB, as AW core depth and AW top depth in the Canada Basin are both greatly influenced by the Beaufort Gyre which affects the two metrics in the same way. The comparatively low correlation between AW core depth and AW top depth in the EEB highlights the care that should be taken when using AW core depth to assess AW layer shoaling here.

Comparing the mean salinity of the AW layer with the AW layer heat content can give an idea of the role that mixing with fresher waters plays in AW heat loss. Figure 14d shows that, while there is a relatively high correlation between these variables in the EEB, the correlation is negligible in the west. This implies that although mixing with fresher waters is important for AW heat loss in the Eurasian Basin - as would be expected given that the AW subducts beneath the cooler, fresh polar waters here, losing a lot of heat - it is not as important in the western Arctic.

In Figure 14e, AW core salinity is compared to AW core potential temperature. In the EEB this reflects what is seen in the integrated AW layer (Figure 14d). In the west however, a stronger (moderate) correlation exists between the AW core data than that between the AW layer data. This could be related to the thermohaline intrusions which spread the warm AW core anomaly into the Canada Basin during the study period (McLaughlin et al., 2009). However it also highlights once again the freshening of the AW core, relative to the AW layer, as it is advected around the Arctic.

7 Conclusion

This study has used all available hydrographic profiles from across the Arctic from the 1970s to 2018 to build a picture of AW in the Arctic Ocean entirely from observations, and to investigate its spatial and temporal variability. Much of the analysis has focused on the properties of the AW core (the depth at which the maximum potential temperature occurs). This was found to be a generally effective and easily detectable metric to assess the heat content of the AW layer. However, the depth of the AW core does not always reflect the depth of the top of the AW layer, particularly in the eastern Arctic, and care must be taken when using temporal trends in AW core properties to assess trends in the AW as a whole - a cooling or increase in salinity of the core does not necessarily translate to a cooling or increase in salinity of the entire AW layer.

In general, as the AW is advected around the Arctic the potential temperature and salinity of its core decrease. Despite freshening, the AW core density increases along its advection pathway. This is partially due to the preferential loss of heat and salt from the top of the AW layer to the fresher, cooler water above through vertical mixing along the AW advection pathway. This likely deepens the core without the AW layer as a whole getting denser - upper AW cools such that the AW core (temperature maximum) is found on deeper (denser) isopycnals. Interaction with dense shelf flows formed by brine rejection during sea-ice formation may also play an important role in the cooling and freshening of the AW core during its advection around the basin.

The evolution of AW has differed between the eastern and western basins of the Arctic. In the Eurasian Basin, AW core temperature and AW heat content increased from 2002–2018, with the former increasing by approximately 0.7 °C during this period. Warm pulses were superimposed upon this trend. Instances of high upper ocean heat content in the east were found to be associated with shallower, fresher AW. In contrast to this, and similar reports in the literature of eastern Arctic Atlantification, the western Arctic saw AW core temperatures decrease from a previous warm peak by approximately 0.1 °C between 2008–2018 (although AW layer heat content increased), and also saw AW heat become more isolated from the surface. This increased isolation was due to Beaufort Gyre intensification which deepened the halocline. These findings suggest the emergence of two different regimes - with AW affecting sea-ice in the east, and Pacific Water influencing sea-ice in the west. This implies that the future evolution of the Eurasian Basin will strongly depend on AW, whereas Pacific Water and the Beaufort Gyre will be the biggest drivers of change in the Canada Basin. This contrasting regional evolution is in agreement with other recent studies, which describe halocline weakening, AW shoaling, and increased sub-Arctic influence in the Eurasian Basin, contrasting with a

freshening and deepening of the surface layer in the Amerasian Basin driven by local atmospheric conditions (Polyakov, Rippeth, et al., 2020; Polyakov, Alkire, et al., 2020).

Despite the limitation of sparse, temporally inhomogeneous oceanographic measurements in the Arctic, pan-Arctic observational analysis can give useful insights into the overall temporal and spatial patterns of heat distribution in the Arctic Ocean. Given the challenges of realistically representing the AW layer in forced ocean-sea-ice and coupled climate models, and the stark regional differences emerging in the Arctic Ocean, the use of pan-Arctic observations for model validation and benchmarking will be essential. Only by combining insight from observations and models will we be able to accurately determine what the future Arctic will look like under a changing climate, which is important both for the region itself as well as for the wider climate system.

Open Research

Profile data used in this study are available from `http://www.whoi.edu/itp` (for ITP data), `https://www.whoi.edu/beaufortgyre` (for BGEP data), `https://uaf-iarc` `.org/nabos` (for NABOS data), and `https://www.ncei.noaa.gov/products/world-ocean` `-database` (for WOD data). The Atlantic Water core data computed for this study are available as an Open Access dataset at the Oxford University Research Archive via `https://` `doi.org/10.5287/bodleian:wxv8GA7Mk`. Note that this dataset includes all mooring data rather than monthly mean mooring data.

Acknowledgments

References

Aksenov, Y., Ivanov, V. V., Nurser, A. J. G., Bacon, S., Polyakov, I. V., Coward, A. C., ... Beszczynska-Moeller, A. (2011). The Arctic Circumpolar Boundary Current. *J. Geophys. Res. Ocean.*, *116*(9). doi: 10.1029/2010JC006637

Anderson, L. G., Bjrrk, G., Jones, E. P., Kattner, G., Koltermann, K. P., Liljeblad, B., ... Swift, J. (1994). Results from the Oden 91 expedition. , *99*, 3273–3283.

Barton, B. I., Lenn, Y. D., & Lique, C. (2018). Observed Atlantification of the Barents Sea Causes the Polar Front to Limit the Expansion of Winter Sea Ice. *J. Phys. Oceanogr.*, *48*(8), 1849–1866. doi: 10.1175/JPO-D-18-0003.1

Bebieva, Y., & Timmermans, M. L. (2017). The relationship between double-diffusive intrusions and staircases in the Arctic Ocean. *J. Phys. Oceanogr.*, *47*(4), 867–878. doi: 10.1175/JPO-D-16-0265.1

Bebieva, Y., & Timmermans, M. L. (2019). Double-Diffusive Layering in the Canada Basin: An Explanation of Along-Layer Temperature and Salinity Gradients. *J. Geophys. Res. Ocean.*, *124*(1), 723–735. doi: 10.1029/2018JC014368

Beszczynska-Moller, A., Fahrbach, E., Schauer, U., & Hansen, E. (2012). Variability in Atlantic water temperature and transport at the entrance to the Arctic Ocean, 1997–2010. *J. Mar. Sci.*, *69*(5), 852–863. doi: 10.1038/278097a0

Carmack, E., Polyakov, I., Padman, L., Fer, I., Hunke, E., Hutchings, J., ... Winsor, P. (2015). Toward quantifying the increasing role of oceanic heat in sea ice loss in the new Arctic. *Bull. Am. Meteorol. Soc.*, *96*(12), 2079–2105. doi: 10.1175/BAMS-D-13-00177.1

Dmitrenko, I. A., Polyakov, I. V., Kirillov, S. A., Timokhov, L. A., Frolov, I. E.,

Sokolov, V. T., ... Walsh, D. (2008). Toward a warmer Arctic Ocean: Spreading of the early 21st century Atlantic water warm anomaly along the Eurasian basin margins. *J. Geophys. Res. Ocean.*, *113*(5), 1–13. doi: 10.1029/2007JC004158

Fer, I. (2009). Weak Vertical Diffusion Allows Maintenance of Cold Halocline in the Central Arctic. *Atmos. Ocean. Sci. Lett.*, *2*(3), 148–152. doi: 10.1080/16742834 .2009.11446789

Ilıcak, M., Drange, H., Wang, Q., Gerdes, R., Aksenov, Y., Bailey, D., ... Yeager, S. G. (2016, apr). An assessment of the Arctic Ocean in a suite of interannual CORE-II simulations. Part III: Hydrography and fluxes. *Ocean Model.*, *100*, 141–161. doi: 10.1016/j.ocemod.2016.02.004

IOC, SCOR, & IAPSO. (2010). *The International Thermodynamic Equation of Seawater-2010: Calculation and Use of Thermodynamic Properties, Manuals Guides.* Paris: UNESCO.

Ivanov, V. V., Alexeev, V. A., Repina, I., Koldunov, N. V., & Smirnov, A. (2012). Tracing Atlantic Water Signature in the Arctic Sea Ice Cover East of Svalbard. *Adv. Meteorol.*, *2012*. doi: 10.1155/2012/201818

Ivanov, V. V., & Golovin, P. N. (2007). Observations and modeling of dense water cascading from the northwestern Laptev Sea shelf. *J. Geophys. Res. Ocean.*, *112*(9), 1–15. doi: 10.1029/2006JC003882

Ivanov, V. V., Shapiro, G. I., Huthnance, J. M., Aleynik, D. L., & Golovin, P. N. (2004). *Cascades of dense water around the world ocean* (Vol. 60) (No. 1). doi: 10.1016/j.pocean.2003.12.002

Jackson, J. M., Williams, W. J., & Carmack, E. C. (2012). Winter sea-ice melt in the Canada Basin, Arctic Ocean. *Geophys. Res. Lett.*, *39*(3), 2–7. doi: 10 .1029/2011GL050219

Karcher, M., Beszczynska-Möller, A., Kauker, F., Gerdes, R., Heyen, S., Rudels, B., & Schauer, U. (2011). Arctic Ocean warming and its consequences for the Denmark Strait overflow. *J. Geophys. Res. Ocean.*, *116*(2), 1–10. doi: 10.1029/2010JC006265

Karcher, M., Smith, J. N., Kauker, F., Gerdes, R., & Smethie, W. M. (2012). Recent changes in Arctic Ocean circulation revealed by iodine-129 observations and modeling. *J. Geophys. Res. Ocean.*, *117*(8), 1–17. doi: 10.1029/2011JC007513

Karcher, M. J., Gerdes, R., Kauker, F., & Köberle, C. (2003). Arctic warming: Evolution and spreading of the 1990s warm event in the Nordic seas and the Arctic Ocean. *J. Geophys. Res. C Ocean.*, *108*(2), 16–1. doi: 10.1029/2001jc001265

Karcher, M. J., & Oberhuber, J. (2002). Pathways and modification of the upper and intermediate waters of the Arctic Ocean. *J. Geophys. Res.*, *107*(C6), 1–13. doi: 10.1029/2000jc000530

Krishfield, R., Toole, J., Proshutinsky, A., & Timmermans, M. L. (2008). Automated Ice-Tethered Profilers for Seawater Observations under Pack Ice in All Seasons. *J. Atmos. Ocean. Technol.*, *25*(11), 2091–2105. doi: 10.1175/2008JTECHO587.1

Kuzmina, N., Rudels, B., Zhurbas, V., & Stipa, T. (2011). On the structure and dynamical features of intrusive layering in the Eurasian Basin in the Arctic Ocean. *J. Geophys. Res. Ocean.*, *116*(12), 1–15. doi: 10.1029/2010JC006920

Ladd, C., Mordy, C. W., Salo, S. A., & Stabeno, P. J. (2016). Winter Water Properties and the Chukchi Polynya. *J. Geophys. Res. Ocean.*, *121*(8), 5516–5534. doi: 10.1038/175238c0

Li, J., Pickart, R. S., Lin, P., Bahr, F., Arrigo, K. R., Juranek, L., & Yang, X. Y. (2020). The Atlantic Water Boundary Current in the Chukchi Borderland and Southern Canada Basin. *J. Geophys. Res. Ocean.*, *125*(8), 1–20. doi: 10.1029/2020JC016197

Lind, S., Ingvaldsen, R. B., & Furevik, T. (2018, jul). Arctic warming hotspot in the

northern Barents Sea linked to declining sea-ice import. *Nat. Clim. Chang.*, *8*(7), 634–639. doi: 10.1038/s41558-018-0205-y

Lique, C., & Johnson, H. L. (2015, nov). Is there any imprint of the wind variability on the Atlantic Water circulation within the Arctic Basin? *Geophys. Res. Lett.*, *42*(22), 9880–9888. doi: 10.1002/2015GL066141

Lique, C., Johnson, H. L., & Davis, P. E. D. (2015, may). On the Interplay between the Circulation in the Surface and the Intermediate Layers of the Arctic Ocean. *J. Phys. Oceanogr.*, *45*(5), 1393–1409. doi: 10.1175/JPO-D-14-0183.1

Lique, C., Johnson, H. L., & Plancherel, Y. (2018). Emergence of deep convection in the Arctic Ocean under a warming climate. *Clim. Dyn.*, *50*(9-10), 3833–3847. doi: 10.1007/s00382-017-3849-9

Lique, C., & Steele, M. (2012, mar). Where can we find a seasonal cycle of the Atlantic water temperature within the Arctic Basin? *J. Geophys. Res. Ocean.*, *117*(C3), n/a–n/a. doi: 10.1029/2011JC007612

Lique, C., Treguier, A. M., Blanke, B., & Grima, N. (2010). On the origins of water masses exported along both sides of Greenland: A Lagrangian model analysis. *J. Geophys. Res. Ocean.*, *115*(5), 1–20. doi: 10.1029/2009JC005316

Luneva, M. V., Ivanov, V. V., Tuzov, F., Aksenov, Y., Harle, J. D., Kelly, S., & Holt, J. T. (2020). Hotspots of Dense Water Cascading in the Arctic Ocean: Implications for the Pacific Water Pathways. *J. Geophys. Res. Ocean.*, *125*(10). doi: 10.1029/2020JC016044

McLaughlin, F. A., Carmack, E. C., Williams, W. J., Zimmermann, S., Shimada, K., & Itoh, M. (2009). Joint effects of boundary currents and thermohaline intrusions on the warming of Atlantic water in the Canada Basin, 1993-2007. *J. Geophys. Res. Ocean.*, *114*(7). doi: 10.1029/2008JC005001

Melling, H., & Moore, R. (1995). Modification of halocline source waters during freezing on the Beaufort Sea shelf: evidence from oxygen isotopes and dissolved nutrients. *Science (80-.).*, *15*(1), 89–113.

Pérez-Hernández, M. D., Pickart, R. S., Torres, D. J., Bahr, F., Sundfjord, A., Ingvaldsen, R., . . . Pavlov, V. (2019). Structure, Transport, and Seasonality of the Atlantic Water Boundary Current North of Svalbard: Results From a Yearlong Mooring Array. *J. Geophys. Res. Ocean.*, *124*(3), 1679–1698. doi: 10.1029/2018JC014759

Perovich, D. K., & Richter-Menge, J. A. (2015). Regional variability in sea ice melt in a changing Arctic. *Philos. Trans. R. Soc. A Math. Phys. Eng. Sci.*, *373*(2045). doi: 10.1098/rsta.2014.0165

Polyakov, I. V., Alekseev, G. V., Timokhov, L. A., Bhatt, U. S., Colony, R. L., Simmons, H. L., . . . Zakharov, V. F. (2004). Variability of the Intermediate Atlantic Water of the Arctic Ocean over the Last 100 Years. *J. Clim.*, *17*(23), 4485–4497. doi: 10.1175/JCLI-3224.1

Polyakov, I. V., Alexeev, V. A., Ashik, I. M., Bacon, S., Beszczynska-Möller, A., Carmack, E. C., . . . Woodgate, R. (2011). Fate of Early 2000s Arctic Warm Water Pulse. *Bull. Am. Meteorol. Soc.*, *92*(5), 561–566. doi: 10.1175/2010BAMS2921.1

Polyakov, I. V., Alkire, M. B., Bluhm, B. A., Brown, K. A., Carmack, E. C., Chierici, M., . . . Wassmann, P. (2020). Borealization of the Arctic Ocean in Response to Anomalous Advection From Sub-Arctic Seas. *Front. Mar. Sci.*, *7*(July). doi: 10.3389/fmars.2020.00491

Polyakov, I. V., Beszczynska, A., Carmack, E. C., Dmitrenko, I. A., Fahrbach, E., Frolov, I. E., . . . Walsh, J. E. (2005). One more step toward a warmer Arctic. *Geophys. Res. Lett.*, *32*(17), 1–4. doi: 10.1029/2005GL023740

Polyakov, I. V., Pnyushkov, A. V., Alkire, M. B., Ashik, I. M., Baumann, T. M., Carmack, E. C., . . . Yulin, A. (2017, apr). Greater role for Atlantic inflows on sea-ice loss in the Eurasian Basin of the Arctic Ocean. *Science (80-.).*, *356*(6335), 285–291. doi: 10.1126/science.aai8204

Polyakov, I. V., Pnyushkov, A. V., & Carmack, E. C. (2018). Stability of the arctic halocline: A new indicator of arctic climate change. *Environ. Res. Lett.*, *13*(12), 125008. doi: 10.1088/1748-9326/aaec1e

Polyakov, I. V., Pnyushkov, A. V., & Timokhov, L. A. (2012, dec). Warming of the Intermediate Atlantic Water of the Arctic Ocean in the 2000s. *J. Clim.*, *25*(23), 8362–8370. doi: 10.1175/JCLI-D-12-00266.1

Polyakov, I. V., Rippeth, T. P., Fer, I., Alkire, M. B., Baumann, T. M., Carmack, E. C., . . . Rember, R. (2020). Weakening of Cold Halocline Layer Exposes Sea Ice to Oceanic Heat in the Eastern Arctic Ocean. *J. Clim.*, *33*(18), 8107–8123. doi: 10.1175/JCLI-D-19-0976.1

Polyakov, I. V., Timokhov, L. A., Alexeev, V. A., Bacon, S., Dmitrenko, I. A., Fortier, L., . . . Toole, J. (2010). Arctic Ocean Warming Contributes to Reduced Polar Ice Cap. *J. Phys. Oceanogr.*, *40*(12), 2743–2756. doi: 10.1175/2010JPO4339.1

Proshutinsky, A., Krishfield, R., Toole, J. M., Timmermans, M. L., Williams, W., Zimmermann, S., . . . Zhao, J. (2019). Analysis of the Beaufort Gyre Freshwater Content in 2003–2018. *J. Geophys. Res. Ocean.*, *124*(12), 9658–9689. doi: 10.1029/2019JC015281

Regan, H. C., Lique, C., & Armitage, T. W. (2019). The Beaufort Gyre Extent, Shape, and Location Between 2003 and 2014 From Satellite Observations. *J. Geophys. Res. Ocean.*, *124*(2), 844–862. doi: 10.1029/2018JC014379

Ruddick, B. (1992). *Intrusive Mixing in a Mediterranean Salt Lens - Intrusion Slopes and Dynamical Mechanisms* (Vol. 22) (No. 11). doi: 10.1175/1520-0485(1992)022⟨1274:IMIAMS⟩2.0.CO;2

Rudels, B. (2015). Arctic Ocean circulation, processes and water masses: A description of observations and ideas with focus on the period prior to the International Polar Year 2007-2009. *Prog. Oceanogr.*, *132*, 22–67. doi: 10.1016/j.pocean.2013.11.006

Schauer, U., Loeng, H., Rudels, B., Ozhigin, V. K., & Dieck, W. (2002). Atlantic Water flow through the Barents and Kara Seas. *Deep. Res. Part I Oceanogr. Res. Pap.*, *49*(12), 2281–2298. doi: 10.1016/S0967-0637(02)00125-5

Shu, Q., Wang, Q., Su, J., Li, X., & Qiao, F. (2019). Assessment of the Atlantic water layer in the Arctic Ocean in CMIP5 climate models. *Clim. Dyn.*, *53*(9-10), 5279–5291. doi: 10.1007/s00382-019-04870-6

Skagseth, Ø., Eldevik, T., Årthun, M., Asbjørnsen, H., Lien, V. S., & Smedsrud, L. H. (2020). Reduced efficiency of the Barents Sea cooling machine. *Nat. Clim. Chang.*, *10*(7), 661–666. doi: 10.1038/s41558-020-0772-6

Spielhagen, R. F., Werner, K., Sørensen, S. A., Kandiano, E., Budeus, G., Husum, K., & Marchitto, T. M. (2011). Enhanced Modern Heat Transfer to the Arctic by Warm Atlantic Water. *Science (80-.).*, *331*(6016), 450–453.

Timmermans, M. L. (2015). The impact of stored solar heat on Arctic sea ice growth. *Geophys. Res. Lett.*, *42*(15), 6399–6406. doi: 10.1002/2015GL064541

Timmermans, M. L., Proshutinsky, A., Golubeva, E., Jackson, J. M., Krishfield, R., McCall, M., . . . Nishino, S. (2014). Mechanisms of Pacific Summer Water variability in the Arctic's Central Canada Basin. *J. Geophys. Res. Ocean.*, *119*, 7523–7548. doi: 10.1038/175238c0

Timmermans, M. L., Toole, J., & Krishfield, R. (2018). Warming of the interior Arctic Ocean linked to sea ice losses at the basin margins. *Sci. Adv.*, *4*(8), 1–7. doi: 10.1126/sciadv.aat6773

Toole, J. M., Krishfield, R. A., Timmermans, M. L., & Proshutinsky, A. (2011). The Ice-Tethered profiler: Argo of the Arctic. *Oceanography*, *24*(3), 126–135. doi: 10.5670/oceanog.2011.64

Turner, J. S. (2010, jan). The Melting of Ice in the Arctic Ocean: The Influence of Double-Diffusive Transport of Heat from Below. *J. Phys. Oceanogr.*, *40*(1), 249–256. doi: 10.1175/2009JPO4279.1

Wefing, A. M., Casacuberta, N., Christl, M., Gruber, N., & Smith, J. N. (2020). Circulation timescales of Atlantic Water in the Arctic Ocean determined from anthropogenic radionuclides. *Ocean Sci.*, *17*(1), 111–129. doi: 10.5194/os-17-111-2021

Woodgate, R. A., Aagaard, K., Muench, R. D., Gunn, J., Björk, G., Rudels, B., . . . Schauer, U. (2001). The Arctic Ocean Boundary Current along the Eurasian slope and the adjacent Lomonosov Ridge: Water mass properties, transports and transformations from moored instruments. *Deep. Res. Part I Oceanogr. Res. Pap.*, *48*(8), 1757–1792. doi: 10.1016/S0967-0637(00)00091-1

Zhang, J., Steele, M., Runciman, K., Dewey, S., Morison, J., Lee, C., . . . Toole, J. (2016, nov). The Beaufort Gyre intensification and stabilization: A model-observation synthesis. *J. Geophys. Res. Ocean.*, *121*(11), 7933–7952. doi: 10.1002/2016JC012196

Zhong, W., & Zhao, J. (2014). Deepening of the Atlantic Water Core in the Canada Basin in 2003-11. *J. Phys. Oceanogr.*, *44*(9), 2353–2369. doi: 10.1175/JPO-D -13-084.1